Materials Advances

ROYAL SOCIETY OF CHEMISTRY

PAPER

View Article Online
View Journal | View Issue

Cite this: *Mater. Adv.*, 2026, 7, 3698

Towards a wearable format for transducing responsive swelling in hydrogels

Rinki Singh, *[a] Dinakaran Thirumalai,[a] Tanya Levingstone[b] and Aoife Morrin *[a]

Responsive hydrogels offer significant promise for wearable biochemical sensing owing to their tuneable chemistries and biocompatible, tissue-like properties. In this study, we demonstrate an impedance configuration as a potentially wearable transduction approach for monitoring swelling dynamics in planar poly(acrylic acid-*co*-*N*,*N*′-methylene-bis-acrylamide) (PAAc-*co*-MBA) hydrogel films. Using surface-mounted gold contact pins, we extract a localised gel resistance parameter (R_{gel}) that was correlated directly with gravimetric swelling measurements, and was shown to provide a quantitative measure of swelling-induced changes. Impedance-based measurements exhibited superior sensitivity compared to the gravimetric measurements, attributed to localised interrogation of hydrogel regions near the electrode interface where equilibration occurs rapidly. The apparent pK_a of the hydrogel, determined from impedance-monitored pH titrations, was measured as 4.1, within 0.4 pH units of the theoretical PAAc value. Systematic optimisation of starting oxidant concentrations revealed that formulations with lower oxidant content achieved optimal mechanical properties suitable for applying to tissue, demonstrating excellent skin adhesion (>350 flexion cycles) whilst maintaining requisite flexibility for conformal wearable applications. To validate tissue interfacing capabilities, hydrogel films were applied to exposed kiwi fruit tissue (pH ∼ 4.0), where the impedance response reflected hydrogen ion diffusion from the tissue into the hydrogel (neutral pH). Concurrent pH mapping and dimensional analysis confirmed ion transport across the tissue-hydrogel interface, demonstrating the material's capacity for real-time monitoring of soft bio-interfaces. These findings establish simplified impedance-transduced PAAc-*co*-MBA hydrogels as promising platforms for next-generation wearable sensors, offering the potential of quantitative, non-invasive monitoring of tissue pH with direct applicability to wearable health monitoring technologies.

Received 29th September 2025,
Accepted 28th February 2026

DOI: 10.1039/d5ma01115a

rsc.li/materials-advances

1. Introduction

Stimuli-responsive hydrogels, composed of crosslinked hydrophilic polymer networks, have great potential as highly versatile sensing materials due to their tuneable composition and inherent ability to undergo reversible volumetric changes in response to target analytes.[1] Alongside advances in hydrogel materials, there is an increasing adoption of wearable devices that monitor physiological parameters, such as temperature, heart rate, and blood pressure.[2] More recently, wearable chemical and biochemical sensing platforms have emerged that require materials capable of interfacing conformally with biological surfaces whilst maintaining sensitivity under physiological conditions.[3]

Hydrogels can be engineered to swell or shrink in response to various stimuli, including pH,[4,5] small ions,[6] organic vapours[7] and biomolecules.[8] Their soft, hydrated, and biocompatible nature makes them particularly attractive for wearable applications, offering mechanical conformity with skin and biological tissues.[9] Their synthetic flexibility further enables high specificity in sensing a diverse range of analytes. Despite these advantages, integrating practical and miniaturisable transduction methods into wearable formats remains a challenge.[10,11] A suitable transduction approach must ensure reliable, sensitive, and reproducible detection of swelling behaviour, whilst being resistant to noise and suitable for compact systems.

Several transduction strategies have been explored for hydrogel-based sensing. Optical,[12] electromechanical,[13] and electrical[14] methods have each demonstrated unique advantages and limitations. Optical approaches, such as hydrogel diffraction gratings, leverage changes in diffracted light due to swelling-induced structural changes.[15,16] Similarly, 2D photonic crystals[17] embedded in responsive hydrogels exhibit analyte-dependent shifts in particle spacing, which can be tracked using relatively simple optical setups.

Electromechanical strategies include piezoelectric microbalances, which detect frequency shifts due to mass changes

[a] *School of Chemical Sciences, Insight Research Ireland Centre for Data Analytics, Dublin City University, D09 V209, Ireland. E-mail: aoife.morrin@dcu.ie, rinkoosingh62@gmail.com*
[b] *School of Mechanical Engineering, Dublin City University, D09 V209, Ireland*

in hydrogels.[13] Ultrasound-based systems have also been demonstrated using acoustic resonator sheets, where swelling and shrinking affect resonance and reflected wave intensity. These approaches have been applied in wearable and subcutaneous formats.[13] Most recent developments include a power transfer method using thin-film polyimide substrates embedded with conductive lines, where hydrogel swelling modulates output voltage.[14] Smartphone imaging of hydrogel shape changes has also been proposed for wearable platforms.[18]

Electrical transduction, particularly impedance-based approaches, remains less explored but offers significant promise for wearable applications due to inherent compatibility with microelectronics and potential for miniaturisation. Swelling-induced conductivity changes in interdigitated electrode (IDE)-coated hydrogels can be detected as variations in impedance or output voltage.[19,20] In one study, a pH-responsive hydrogel sensor demonstrated reliable and sensitive detection of acidosis-relevant pH shifts through impedance measurements, highlighting its promise for minimally invasive monitoring of tissue acidosis.[21] The same group developed a covalent adhesion strategy for responsive poly(2-hydroxyethyl methacrylate-*co*-poly(ethylene glycol) methacrylate-*co*-hexyl methacrylate) hydrogels on gold–glass microelectrode chips using acryloyl-poly(ethylene glycol)-3500 *n*-hydroxysuccinimide surface functionalisation. Impedance spectroscopy revealed diffusion-driven swelling kinetics with ~30 min equilibration, supporting their use in real-time biosensing applications.[22]

Impedance spectroscopy is widely employed in chemical and biochemical sensing due to its sensitivity, reliability, and ease of integration with microelectronics.[23] Our group has demonstrated its utility in various hydrogel systems, including interdigitated electrodes,[19,24,25] temporary tattoo-based sensors for polyethylene glycol-based hydrogels,[26] and enzyme-functionalised hydrogels applied to carbon cloth for glucose sensing *via* pH-induced swelling.[22] This system employed a three-electrode cell configuration and demonstrated high sensitivity (0.28 to 1.11 mM). Another study using impedimetric transduction demonstrated hydrogel-functionalised microelectrodes for quantifying species, including DNA and enzymes,[27] establishing the potential of impedance as a simple, versatile, and configurable method of transduction.

The novelty of the present work lies in the integration of a two-electrode cell configuration for integration within a wearable format for transducing the swelling of a mechanically optimised pH responsive PAAc-*co*-MBA hydrogel. Unlike prior studies employing microfabricated interdigitated electrodes, where swelling-induced ionic conductivity changes across patterned gold IDE fingers are monitored as impedance or voltage shifts.[19] Similarly, bulk conductivity transducers incorporate hydrogels into conductimetric cells where changes in ion mobility throughout the entire hydrogel volume alter the measured resistance.[20,21] These systems rely on microfabricated electrodes, embedded metal lines, or enclosed sensing chambers, and they probe either micrometre scale hydrogel coatings or the entire bulk hydrogel, limiting their suitability for soft, conformal wearable integration. In contrast, our surface-mounted configuration uses two spring-loaded gold contact pins, enabling direct interrogation of the hydrogel surface and extraction of a quantitative impedance parameter (R_{gel}). By comparing R_{gel} to bulk gravimetric swelling (G_{gel}), we observe distinctions between local interfacial and bulk hydration, offering mechanistic insight not previously demonstrated. Moreover, we show that this impedance method can directly track pH-driven swelling at a soft biological interface, using kiwi tissue as a model substrate, underscoring its potential for non-invasive biochemical monitoring on soft tissue interfaces. This approach provides a new pathway for wearable hydrogel-based biosensing, distinct from prior hydrogel synthesis and transduction strategies.

Poly(acrylic acid) (PAAc)-based hydrogels were selected in this work due to their strong previously reported skin-adhesive nature,[28] good swelling capability[29] and ionisability. These characteristics motivated us to investigate impedance based swelling transduction of these materials and wearable biochemical sensing. PAAc contains a high density of ionisable carboxylic acid (–COOH) groups that undergoes reversible dissociation near their pK_a (~4.5),[30–32] producing pronounced pH dependent variations in ionic conductivity and swelling. This pK_a closely overlaps with the physiologically relevant pH range of skin and soft tissue (pH ~4–5.8),[33] enabling high sensitivity to biologically meaningful pH. In addition, PAAc based hydrogels exhibit hydrogen bonding with hydroxyl and amine groups on the skin surface mediated adhesion[34,35] and excellent biocompatibility,[36] which are essential for stable interfacing with human skin. Furthermore, crosslinking with *N,N′*-methylene-bis-acrylamide (MBA) yields mechanically robust yet highly conformable networks.

In this study, we aim to establish impedance spectroscopy as a simple transduction method for monitoring swelling behaviour in responsive hydrogels for wearable applications. We investigate the use of a simple two-electrode cell configuration to quantify swelling in poly(acrylic acid-*co*-*N,N′*-methylene-bis-acrylamide) (PAAc-*co*-MBA) hydrogels and assess how both swelling conditions and hydrogel formulation parameters influence impedance responses. The work further examines the mechanical strength, adhesive performance, and pH sensitivity of the hydrogels to determine their suitability for interfacing with the skin. As part of these objectives, we also seek to evaluate the applicability of the hydrogels for *in-situ* monitoring by interfacing them with soft fruit tissue, enabling assessment of their ability to respond impedimetrically to local pH environments. By establishing these capabilities, the study aims to determine the potential of these soft, responsive hydrogel materials for future development as wearable biochemical sensing platforms.

2. Methods

2.1. Materials

All standard reagents, including acrylic acid (AAc, 79-10-7), ammonium persulfate (APS, 7727-54-0), *N,N′*-methylenebisacrylamide (MBA, 110-26-9), and *N,N,N′N′* tetramethylethylenediamine

(TEMED, 110-18-9), were purchased from Merck (Ireland). Hydrochloric acid (7647-01-0), sodium hydroxide (1310-73-2), and potassium chloride (7447-40-7) were also purchased from Merck (Ireland). For the electrode assembly, RS PRO clear plastic sheets (769-8733) were purchased from Maplin Electronics. Mill Max spring-loaded contacts (gold-plated copper alloy, 0906-4-15-20-75-14-11-0) were purchased from Farnell Components (Ireland). Kiwi fruits were purchased from a local grocery store in Dublin.

2.2. Preparation of hydrogel films

PAAc-*co*-MBA hydrogels were prepared *via* one-pot free radical polymerisation[29,37] (Scheme 1), and the synthesis protocol is shown in Fig. S1. A solution of AAc (20% v/v, unless otherwise specified), TEMED (0.83%), and MBA (1.5% w/v, unless otherwise specified) was prepared in deionised (DI) water and stirred at room temperature for 20 min. APS (8.8% w/v, unless otherwise specified) was then added, and the solution was stirred for an additional 20 min.

To prepare hydrogel films, a 10 mL aliquot of this solution was transferred into a glass Petri-dish (diameter: 6.5 cm) and placed on a hot plate at 37 °C for 5–10 s to initiate polymerisation. The resulting hydrogel discs (4 mm in depth) were removed, rinsed with DI water, and gently blotted dry with a paper towel. Each hydrogel disc was divided into 4 quadrants using a scalpel and used for testing.

2.3. Tracking hydrogel swelling

Hydrogel swelling was monitored using both gravimetry and electrochemical impedance spectroscopy (EIS). Gravimetric measurements were conducted using a standard laboratory mass balance (Sartorius QUINTIX224-1S, Sartorius Lab Instruments, Germany), while impedance measurements were collected using a CH660C potentiostat.

For gravimetric analysis, prepared hydrogel quadrants were first weighed to obtain their initial mass (2 g) (W_i). The hydrogels were then immersed in a specified solute solution (100 mL). After a pre-determined period, the hydrogels were removed, gently blotted dry with a paper towel, and re-weighed to obtain the final mass (W_f). The change in percentage swelling transduced *via* gravimetry ($\Delta\%G_{gel}$) was calculated using eqn (1).[19,39]

$$\Delta\%G_{gel} = \frac{W_f - W_i}{W_i} \times 100 \quad (1)$$

where W_i is the initial weight of the hydrogel (g) before placing it into the solution, and W_f is the final weight of the hydrogel following immersion in solution (g) for a specified period. Hydrogel quadrants were re-immersed in the solution, and the process was repeated at specified time points as needed.

For impedance measurements, a plastic board (dimensions: 5.4 cm × 2.5 cm) mounted with two spring-loaded gold contact pins (7 mm apart) was gently placed onto the surface of a hydrogel quadrant and secured using tape (Fig. S2). A frequency sweep (0.1 to 100 000 Hz) was applied with an amplitude of 0.01 V at a set potential of 0 V, unless otherwise specified. A measure of the hydrogel's resistance was obtained from a fitted equivalent circuit model and recorded as R_i. The hydrogel was then immersed in a specified solution (100 mL), and after a pre-determined duration, it was removed, blotted dry, and re-measured under the same electrical conditions to obtain a final resistance R_f. The change in percentage swelling transduced *via* impedance ($\Delta\%R_{gel}$) was calculated using eqn (2).

$$\%\Delta R_{gel} = \frac{R_f - R_i}{R_i} \times 100 \quad (2)$$

where, R_i is the initial resistance of the hydrogel before immersion, and R_f is the resistance after immersion in the solute's solution for a specified duration. As with the gravimetric analysis, hydrogel quadrants were re-immersed and measured at subsequent defined time points as required.

2.3.1. Transduction of hydrogel swelling in response to solution ionic strength. To investigate whether impedance measurements could be employed to track hydrogel swelling in response to varying solution ionic strength (IS), aqueous solutions containing different concentrations of potassium chloride (KCl) were prepared to adjust the IS of the swelling medium. Hydrogel quadrants were prepared as described above and immersed in KCl solutions of increasing IS (0.001 M, 0.01 M, and 0.1 M) at room temperature. Each immersion step was maintained for 300 min to ensure equilibrium swelling. After each step, the hydrogel was removed from solution, blotted dry gently with a Kimwipe, and gravimetric measurements performed to quantify hydrogel swelling (G_{gel}), followed by impedance spectroscopy to extract the gel resistance (R_{gel}). This process was repeated sequentially across the entire IS range. All experiments were conducted with a minimum of three replicates for each IS condition, and results are presented as mean ± standard deviation.

2.3.2. Influence of crosslinker and oxidant concentrations on hydrogel swelling and impedance responses. To investigate the influence of formulation parameters on hydrogel swelling and impedance characteristics, PAAc-*co*-MBA hydrogels were synthesised with varying concentrations of cross-linker, *N*,*N*′-methylenebisacrylamide (MBA), and oxidant, ammonium persulfate (APS), while keeping the monomer concentration constant. MBA concentrations of 0.5%, 1.0% and 2.0% (w/w

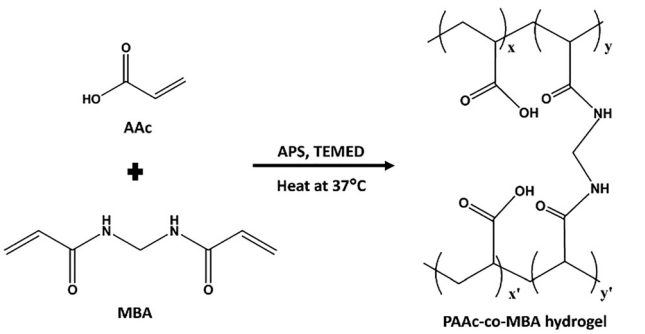

Scheme 1 Schematic of the free radical polymerisation reaction used for the preparation of PAAc-*co*-MBA hydrogels.[38] *x* and *x*′ correspond to polymerised acrylic acid units, and y and y′ correspond to crosslinked segments from MBA, which form bridges between polymer chains.

relative to monomer) and APS concentrations of 1.5%, 2.3%, and 8.8% (w/w relative to monomer) were investigated.

Hydrogel quadrants prepared with each formulation were immersed in DI water at room temperature, and swelling was monitored over time. Gravimetric measures of swelling (G_{gel}) were collected by weighing the hydrogels at pre-determined intervals following gentle blotting. Impedance measurements (R_{gel}) were carried out in parallel using the same procedure as described above in Methods Section 2.4. All experiments were performed in triplicate for each formulation, and results are reported as mean ± standard deviation.

2.3.3. Transduction of hydrogel swelling in response to solution pH. To investigate transduction of hydrogel swelling in response to solution pH, aqueous solutions across a range of pH values from acidic to alkaline at room temperature were prepared from HCl (0.01 M) and NaOH (0.01 M). Initial gravimetric and impedance measurements were performed on hydrogel quadrants as described above. The hydrogels were then sequentially immersed in solutions of increasing pH values (pH 2.0, 4.0, 5.0, 6.0, and 8.0), each for a period of 120 min. After each immersion step, gravimetric and impedance measurements were both collected. This process was continued until the hydrogel quadrant had been exposed to all specified solution pH environments. All experiments were performed in triplicate, and results are reported as mean ± standard deviation.

2.4. Hydrogel characterisation

Attenuated Total Reflectance-Fourier Transform Infrared (ATR-FTIR) (PerkinElmer, Spectrum II) spectra were collected for PAAc-*co*-MBA hydrogels (20% AAc, 1.5% MBA, 8.8% APS), over the range 4000–400 cm^{-1} (Fig. S3). Tensile measurements were performed using a Zwick/Roell Z005 universal testing machine (Zwick/Roell, Germany) equipped with a 500 N load cell. Briefly, dumbbell-shaped hydrogel film samples (20% AAc, 0.15% MBA, 1.5–8.8% APS) with dimensions of 13 mm (length) × 2.6 mm (width) × 2 mm (thickness) were prepared and secured in grips. Testing was conducted at a rate of 0.1 mm s^{-1} in air at room temperature, and samples were stretched to failure. The elongation at break was recorded, and the elastic modulus was calculated from the linear region of the corresponding stress–strain curve.

For the skin adhesion study, hydrogels (20% AAc, 0.15% MBA, 1.5% APS) were cut using a sterile blade into strips measuring 40 mm × 0.5 mm × 2 mm. Informed consent was received from the volunteer participant. Each hydrogel strip was applied to the index finger of the volunteer under ambient conditions, and the number of complete finger flexes until detachment or visible failure was counted.

2.5. Transduction of hydrogel swelling on tissue-mimicking substrate

Hydrogels were applied to kiwi fruit tissue to investigate tracking pH at a tissue interface. The fruits were sliced open to expose the internal tissue, and the pH of the freshly cut surface was measured using pH test strips. In a typical experiment, hydrogel films were prepared as described in Methods Section 2.2, except that 500 μL only of the precursor solution was drop-cast onto a glass slide and allowed to cure at 37 °C to obtain thin hydrogel films (20% AAc, 0.15% MBA, 1.5% APS; dimensions: 3 cm (length) × 2.4 cm (width) × 0.5 mm (depth)). The films were equilibrated in DI water for 2 h to reach swelling equilibrium and were then immediately placed onto the exposed kiwi tissue and maintained at room temperature for ∼2800 s. Impedance spectra were repeatedly recorded at ∼130 s intervals using the conditions in Methods Section 2.3. At defined time points, the hydrogel film was carefully removed from the kiwi surface, and universal indicator paper was gently applied to the outer surface of the hydrogel and to the underlying kiwi surface to colorimetrically assess changes to the bulk hydrogel pH and to verify kiwi tissue pH throughout the experiment. A control experiment was conducted under identical conditions but on a glass slide in place of the kiwi using the same equilibrated hydrogel film preparation to evaluate impedance stability in the absence of tissue. In both test and control conditions, hydrogel dimensional changes were measured against a standard ruler from collected images taken with a mobile phone at specific time intervals.

3. Results & discussion

3.1. Investigation of impedance for tracking hydrogel swelling

Transducing hydrogel swelling *via* impedance has been previously explored using various methodologies, as discussed earlier.[19,40,41] To evaluate the potential of the setup described herefor monitoring swelling *via* impedance, impedance spectra were collected on freshly prepared PAAc-*co*-MBA hydrogels using spring-loaded gold contact pins applied to the hydrogel surface (Fig. S2). Prior to selecting a representative hydrogel composition for impedance spectrum analysis, a comparative gravimetric study was performed on PAAc-*co*-MBA hydrogels prepared with 10%, 20% and 30% AAc at fixed 1.5% MBA and 8.8% APS concentrations. The corresponding gravimetric profiles ($\Delta\%G_{gel}$) are provided in the supporting information (Fig. S4). Hydrogels prepared with 10% AAc exhibited excessively high swelling, which compromised their dimensional stability, while hydrogels prepared with 30% AAc showed comparatively low swelling capacity, limiting sensitivity. In contrast, hydrogels prepared with 20% AAc demonstrated a favourable balance between high swelling responsiveness and mechanical stability. Based on this data, the 20% AAc, 1.5% MBA, 8.8% APS formulation was selected as the representative composition for impedance spectrum analysis shown in Fig. 2. The resulting Nyquist plot (Fig. 2a) displayed two well-defined regions: a partial semi-circle at high frequencies and a non-vertical spike at lower frequencies. The high-frequency semi-circle corresponds to the time constant of the bulk hydrogel material. The low-frequency feature likely represents a second time constant associated with the gold pin-hydrogel surface interface, though it may also include additional contributions such as polarisation effects. To distinguish the individual components, the data were fitted using a proposed equivalent

Fig. 1 Proposed equivalent circuit model.

circuit model.[19] The equivalent circuit model in Fig. 1 includes a constant phase element (CPE1) in parallel with a resistor (R_{gel}), representing the bulk hydrogel's impedance. The value of R_{gel} for a freshly prepared hydrogel was approx. 135 Ohm (Fig. 1a, inset), and this extracted parameter was investigated in this work as a quantitative measure of physical swelling of the hydrogel. In the model, this high-frequency element is in series with a second constant phase element (CPE2) and resistor ($R_{elec\text{-}inter}$) representing the electrode interface with the hydrogel. The use of CPEs in the model accounts for non-ideal capacitive behaviour, which in this case likely arises from non-uniform current distributions within the hydrogel.

To assess the potential of R_{gel} for monitoring hydrogel swelling, a series of impedance spectra and corresponding gravimetric measurements were collected on hydrogel quadrants at pre-determined times after immersion in DI water (0–300 min) (Fig. 2b and c, Table S1). It can be seen that as swelling time increased, the weight of the hydrogel increased due to water uptake by the hydrogel. A corresponding increase in R_{gel} with increasing swelling time is also observed. The increase in R_{gel} reflects a volumetric expansion of the aqueous compartment of the hydrogel, rather than structural changes in the polymer network itself. Fig. 1c shows that at early time points (<40 min), changes in $\Delta\%R_{gel}$ and gravimetry ($\Delta\%G_{gel}$) were similar in magnitude. However, as swelling time increased, $\Delta\%R_{gel}$ increased at a faster rate than $\Delta\%G_{gel}$ and ultimately reached a higher relative change over the 300 min of the experiment. This sensitivity difference over this timescale is likely due to the localised nature of the impedance measurement, which interrogates a highly localised volume of hydrogel directly beneath the electrode-hydrogel interface. This confined volume, which is close to the surface, will swell more rapidly as it has a short diffusion path and will reach swelling equilibrium more rapidly than the bulk volume of the hydrogel, which is what is interrogated gravimetrically. It is important to note that the hydrogel resistance parameter R_{gel} does not represent a direct measure of the bulk volumetric swelling. Instead R_{gel} should be interpreted as a phenomenological proxy that reflects local changes in hydration state, ionic concentration, and ion mobility within the hydrogel region immediately beneath the electrode-hydrogel interface. Because impedance measurements interrogate a spatially confined interfacial volume, R_{gel} is inherently more sensitive to local physiological changes occurring near the surface rather than to the bulk swelling of the entire hydrogel. Accordingly, the relationship observed is expected, with impedance measurements providing enhanced sensitivity to early-stage and interfacial swelling processes.

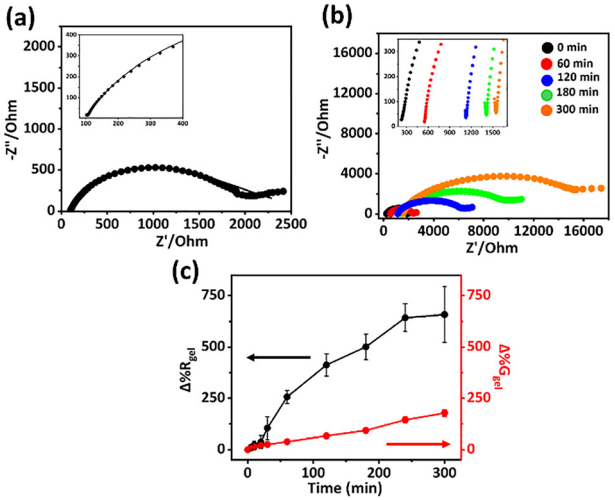

Fig. 2 (a) Nyquist plot and fitted model (see Table S2) for a freshly prepared hydrogel quadrant. Inset (top left): shows the magnification of the high frequency region, (b) Nyquist plots collected at various swelling time points (0–300 min), and (c) $\Delta\%R_{gel}$ and $\Delta\%G_{gel}$ over swelling time for hydrogel quadrants (n = 3). PAAc-*co*-MBA hydrogel composition: 20% AAc, 1.5% MBA, 8.8% APS.

To investigate whether the extracted R_{gel} parameter could be utilised to track swelling in response to swelling solution ionic strength (IS), hydrogels were immersed in solutions of KCl of varying concentrations and allowed to reach equilibrium swelling. Gravimetric and impedance measurements were collected on the equilibrated hydrogels according to Methods. $\Delta\%R_{gel}$ and $\Delta\%G_{gel}$ values were extracted and plotted against swelling solution IS (Fig. 3). Both $\Delta\%G_{gel}$ and $\Delta\%R_{gel}$ were observed to decrease with increasing IS (Fig. 3). In the case of the gravimetric measurement, this is expected, as the increasing IS leads to progressive deswelling due to the uptake of the counter-ions (K^+ in this case), which electrostatically screen the repulsion between the carboxylate groups along the backbone of the polymer.[42,43] In the case of the resistance measurements, the corresponding Cl^- co-ion uptake will lead to a increased conductivity of the aqueous compartment of the hydrogel, which can explain the decrease in $\Delta\%R_{gel}$. Although $\Delta\%R_{gel}$ follows the same trend as $\Delta\%G_{gel}$, it exhibits a notably smaller

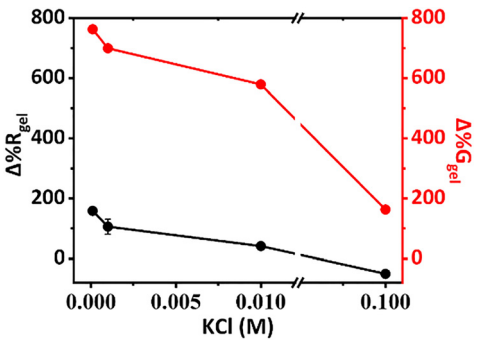

Fig. 3 $\Delta\%R_{gel}$ (black) and $\Delta\%G_{gel}$ (red) as a function of solution IS. Data were collected after a swelling time of 300 min (n = 3). PAAc-*co*-MBA hydrogel composition: 20% AAc, 0.15% MBA, 1.5% APS.

magnitude of change over the IS range studied. The reasons for this are likely complex and not fully clear, but the partial exclusion of the Cl^- co-ions during swelling due to repulsive effects may partially account for the disparity. The corresponding Donnan potential is important to consider as it will generate across the hydrogel-solution interface in the swelling solution but will decay upon removal from solution, leading to a reduced surface conductivity and a corresponding redistribution of the counter- and co-ions in the hydrogel, which will contribute to the net change in resistance.

In hydrogel systems intended to adhere and conform to dynamic surfaces such as skin tissue, it is essential to maintain a balance between elastic and adhesive character. Typically, increased elasticity results in reduced adhesion.[37] The concentrations of cross-linker and oxidant, relative to monomer, are known to modulate both the elastic and adhesive properties of PAAc-*co*-MBA hydrogels[37] and thus the impact of cross-linker (MBA) and oxidant (APS) concentrations was examined (Fig. 4a–d; Table S3). The effect of starting MBA concentration on $\Delta\%R_{gel}$ and $\Delta\%G_{gel}$ as a function of time is shown in Fig. 4a and b. Both R_{gel} and G_{gel} decreased with increasing crosslinking as expected. Interestingly, the kinetics observed were dependent on the transduction method used, attributed largely to the different volumes of hydrogel being interrogated by each technique as discussed earlier. In the case of impedance, the process of imbibing solution into the localised volume of hydrogel directly underneath the surface-applied gold pin electrodes is what is being interrogated. The localised swelling of this confined volume of hydrogel reaches equilibrium early (~300 min), ahead of the bulk reaching swelling equilibrium, which is what is being tracked gravimetrically, and requires significantly longer, up to ~3000 min (Fig. S5).

Varying the oxidant concentration was also evaluated. PAAc-*co*-MBA hydrogels prepared from lower oxidant concentrations (1.5 and 2.3% APS) appeared transparent, whereas hydrogels prepared from a higher oxidant concentration (8.8%) appeared translucent (Fig. S6). A high APS concentration will result in a faster initiation rate and accelerated polymerisation.[44] This promotes the formation of large numbers of lower molecular weight chains[44,45] and thus a much more aggregated network, which explains the observed translucency.[46]

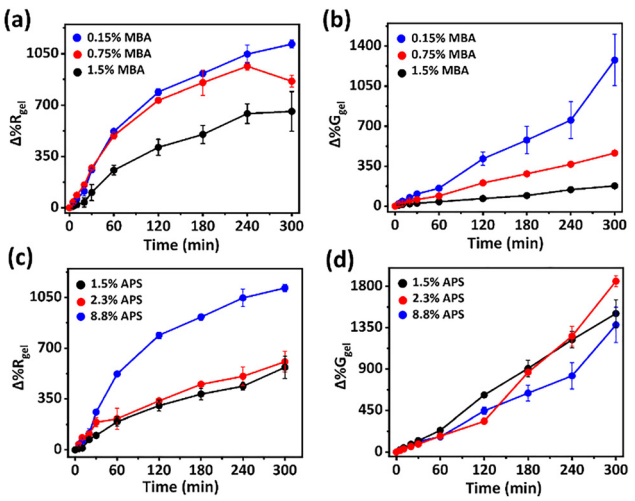

Fig. 4 (a) $\Delta\%R_{gel}$ and (b) $\Delta\%G_{gel}$ over swelling time for hydrogel quadrants (20% AAc, 8.8% APS) (n = 3) with varying MBA concentration; and (c) $\Delta\%R_{gel}$ and (d) $\Delta\%G_{gel}$ over swelling time for hydrogel quadrants (20% AAc, 0.15% MBA) (n = 3) with varying APS concentrations.

While swelling kinetic differences observed with gravimetry are largely similar across oxidant concentrations (Fig. 4d), there is a minor effect noted for higher oxidant concentrations whereby lower swelling is observed for 8.8% APS, most apparent at the latter timepoints. This is consistent with a reduced rate of solution uptake in these hydrogels, and we attribute this to the high level of polymer aggregation present. However, it is anticipated that final equilibration would lead to complete aggregate dissolution and homogeneous water distribution, resulting in equilibrium swelling consistent with that seen at lower oxidant concentrations.

The impact of high oxidant concentration is more pronounced for R_{gel} (Fig. 4c), where hydrogels prepared with the highest concentration of APS (8.8%) underwent the most significant change, approximately twice as large a response after 60 min of swelling time compared to those prepared with lower APS concentrations. This dramatic overall change in resistance at high oxidant concentration is attributed to the initial presence of dense polymer aggregates which result in some exclusion of water and a high ionic conductivity due to the concentrated population of ionic carboxylate groups.[47] Upon solution uptake, internal re-organisation of the polymer aggregates and their at least partial dissolution, leads to a dilution of the ionic charge accounting for this larger net increase in resistance relative to the transparent hydrogels prepared at lower APS concentrations. The hydrogel resistance parameter (R_{gel}) reported throughout this work is the key impedance derived metric used as a quantitative measure of the physical swelling behaviour of the hydrogel. The changes in R_{gel} directly reflect formulation dependent variations in ionic conductivity arising from swelling induced changes in the hydrogel. To illustrate the consistency of this parameter across different formulations, representative Nyquist plots obtained for hydrogels prepared with different APS concentrations are provided in Supporting Information (Fig. S7). These spectra demonstrate that R_{gel} remains well-defined and reproducible parameter across oxidant concentrations, while its magnitude varies systematically with formulation. Overall, these results demonstrate R_{gel} as a sensitive parameter for monitoring hydrogel swelling processes and can offer enhanced spatial resolution and responsiveness to structural heterogeneities that are not as readily observable through bulk gravimetric analysis.

While the hydrogel formulations investigated here were selected based on initial screening to balance swelling responsiveness, mechanical stability, and impedance response reproducibility, we acknowledge that more extensive optimisation of monomer, crosslinker, and oxidant starting concentrations could further influence the quantitative correspondence between impedance derived (R_{gel}) and gravimetric (G_{gel}) measures of swelling.

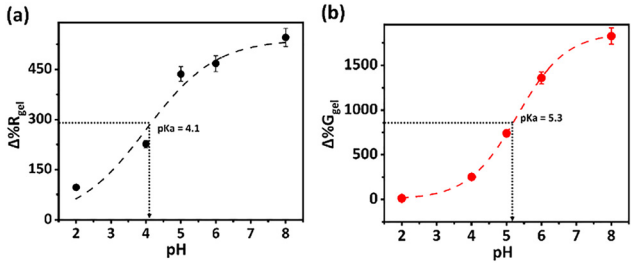

Fig. 5 (a) $\Delta\%R_{gel}$ and (b) $\Delta\%G_{gel}$ as a function of solute pH, IS 0.01 M. Data were collected after a swelling time of 120 min. The data are fitted by the logistic sigmoidal growth model; all measurements were performed in triplicate (n = 3) (eqn (S1), Table S4). PAAc-*co*-MBA hydrogel composition: 20% AAc, 0.15% MBA, 1.5% APS.

Hydrogel swelling in response to solution pH was also investigated using impedance as described in Methods Section 2.3. Fig. 5a and b show $\Delta\%R_{gel}$ and $\Delta\%G_{gel}$ values as a function of pH (IS 0.01 M) after 120 min swelling time. Both impedance and gravimetric measurements exhibited broadly consistent response behaviours with increasing pH (Fig. 5), which can be attributed to pH-dependent electrostatic repulsion arising from the ionisation state of the pendant carboxyl group.[48] Both $\Delta\%R_{gel}$ and $\Delta\%G_{gel}$ follow the behaviour of weak acid titration curves. Accordingly, a sigmoidal growth model (eqn (S1)) was fitted to the data (Table S4), with the inflection point (x_c) of the curve corresponding to the apparent pK_a. Based on these fits, the pK_a values estimated from the impedimetric and gravimetric data were 4.1 and 5.3, respectively, while the literature pK_a for PAAc is $\sim$4.5.[30–32] While both experimental pK_a parameter values likely include significant error, there is a difference of $>$1 pH unit between them, indicating methodological differences. The lower pK_a value derived from R_{gel} measurements may be attributed to the presence of residual unreacted free acrylic acid monomer in the hydrogel, which has a known pK_a of 4.2.[49] The presence of this species could influence hydrogel impedance but may be only a negligible contribution to bulk swelling as measured gravimetrically. It should be emphasized that the pK_a reported here are apparent and inherently dependent on the measurement technique. Gravimetric measurements reflect bulk hydrogel swelling behaviour, whereas the impedance derived parameter R_{gel} probes a highly localised region near the electrode-hydrogel interface, where ionisation, ionic redistribution, and hydration equilibrate more rapidly and non-uniformly. As a result, a shift in the apparent pK_a extracted for hydrogels does not necessarily indicate compositional artefacts. Residual unreacted acrylic acid monomer may further influence the local ionic conductivity response captured by impedance without significantly affecting bulk swelling, suggesting that the observed pK_a offset arises from a combined effect of local interfacial interrogation and potential residual monomer contributions.

Impedance and gravimetric measurements interrogate different physical aspects of the hydrogel and therefore provide complementary information. Impedance spectroscopy probes a localised region at the electrode-hydrogel interface, where changes in hydration state and ionic mobility occur rapidly, while gravimetric measurements capture the bulk swelling of the hydrogel. Accordingly, differences in swelling magnitude and apparent pK_a values reflect the distinct spatial sensitivities of the two techniques rather than inconsistencies in the hydrogel response.

Overall, these investigations highlight the sensitivity of impedance measurement to localised physicochemical changes within the hydrogel environment, showing its potential as a technique for monitoring responsive hydrogel swelling behaviour.

3.2. Mechanical properties of responsive hydrogels

For hydrogel-based wearable sensors, appropriate mechanical properties are essential. By integrating mechanical robustness and skin adhesion, responsive hydrogels can serve as effective interfaces for wearable applications.[34,50] To evaluate how mechanical properties depend on the initial PAAc-*co*-MBA hydrogel formulation, tensile testing was conducted to investigate the influence of oxidant concentration (Fig. 6), as the oxidant is known to impact polymer chain length[51] and, consequently, the stiffness of the resulting material.

As shown in Fig. 6a and b (and Fig. S8), increasing the oxidant concentration led to higher elastic modulus values and reduced elongation at break. A higher elastic modulus indicates a stiffer material that resists deformation under applied stress, while reduced elongation signifies a decrease in flexibility.[52] The mechanical behaviour observed aligns with the understanding that higher oxidant concentrations promote shorter polymer chain lengths, thereby increasing crosslink density and stiffness as discussed above.

In terms of skin adhesion, all hydrogels demonstrated good initial adhesion, which is attributed to the presence of pendant

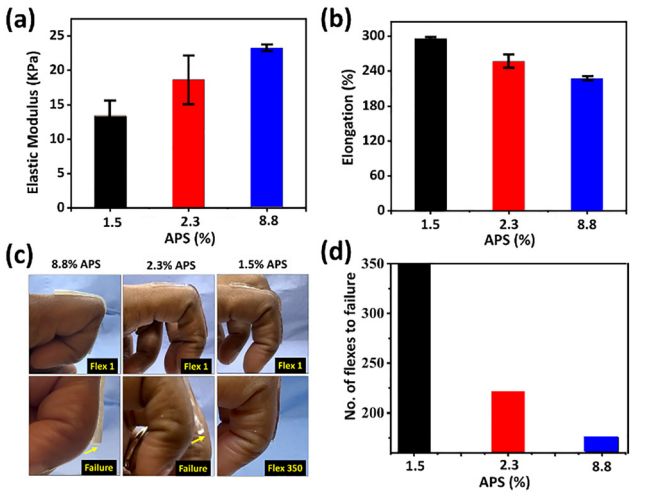

Fig. 6 (a) Elastic modulus and (b) % elongation at break for PAAc-*co*-MBA hydrogels with varying APS concentrations (n = 3); (c) images of the different hydrogel films on a volunteer's index finger after undergoing flexing from 0° to 90°, after 1 flex (top) and after a number of flexes to failure point (bottom), and (d) number of flexes to failure point as a function of %APS. PAAc-*co*-MBA hydrogel composition: 20% AAc, 0.15% MBA.

carboxyl groups that can form hydrogen bonds with hydroxyl and amine groups on the skin surface.[34,35] To evaluate adhesion performance under dynamic mechanical stress, thin hydrogel strips were applied to the top of the index finger of a participant (Fig. 6c), and the finger was repeatedly flexed from 0° to 90°. The number of flexes before significant delamination (or adhesion failure) is recorded. Fig. 6c and d show that the hydrogel strip prepared with the lowest oxidant concentration (1.5% APS) maintained the strong adhesion with skin under mechanical stress, sustaining up to 350 flexes without failure. In contrast, hydrogels with higher oxidant concentrations exhibited reduced adhesion, as indicated by earlier failure during repeated flexion. This result is attributed to the more favourable mechanical profile of the low oxidant hydrogel, which combines lower stiffness (elastic modulus) with higher stretchability (elongation), thus promoting better conformity to dynamic soft tissue surfaces.

3.3. Investigating impedance for tracking hydrogel swelling in response to kiwi tissue pH

Numerous physiological processes in skin tissue have the potential to be monitored using wearable biochemical sensors, *e.g.*, changes to cellular growth,[53] skin barrier function,[26] skin and wound infections,[54] and healing processes.[55] Hydrogels represent promising materials for these applications due to their tuneable volumetric responses to biochemical stimuli, enabled by tailored polymer chemistries.[56–58] To demonstrate the applicability of the mechanically optimised PAAc-*co*-MBA hydrogel for *in-situ* tissue monitoring, we investigated whether films of this hydrogel, when interfaced with kiwi fruit tissue, could respond to the local tissue pH. Exposed kiwi fruit was selected as a tissue for this study owing to its naturally acidic internal tissue environment (~pH 4.0). Although skin surface pH can extend toward higher values (~5.5–6.0) depending on anatomical site and physiological state, acidic conditions approaching pH ~4.0 are well established within the normal skin acid mantle and therefore represent a physiologically relevant regime for evaluating interfacial pH-responsive hydrogel behaviour.[59] While kiwi fruit is not intended as a physiological analogue of human skin, it provides a soft, hydrated, and diffusion permissive tissue substrate suitable for evaluating interfacial pH driven hydrogel swelling under controlled conditions. Fruit tissues (such as banana, oranges and watermelon)[60–62] are used in biomedical and bioelectrochemical research as experimental phantoms where hydration, compliance, and ionic diffusion rather than full anatomical fidelity are the primary functional requirements. In this context, the kiwi experiment serves as a proof-of-concept demonstration of the ability of the impedance transduction method to capture real time pH induced swelling at a soft tissue interface.

For this investigation, a DI water equilibrated hydrogel film (~1.5 mm depth) was applied to the exposed surface of a freshly sliced kiwi, and a series of consecutive impedance spectra were recorded at ~130 s intervals (Fig. 7a), as described in Methods Section 2.5. The hydrogel film interfaced with the kiwi showed a substantial decrease in $\Delta\%R_{gel}$ over time, where

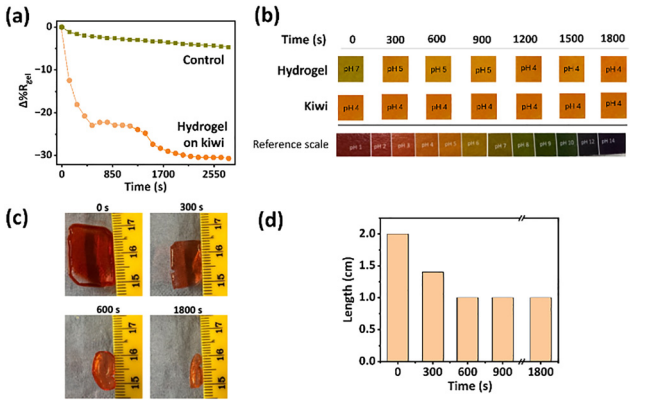

Fig. 7 (a) $\Delta\%R_{gel}$ collected over 3000 s (1 measurement every ~130 s) for hydrogel films interfaced with exposed internal kiwi fruit tissue (~pH 4.0) and without tissue interfacing (control), (b) pH indicator strip images showing transition of hydrogel outer surface pH from 7.0 to 4.0 due to hydrogen ion diffusion from the kiwi. The kiwi surface remained stable at pH 4.0, and (c) Time-lapse images of hydrogel length (cm) at various time points (0–1800 s). (d) The bar graph visualises the length dimension over time. PAAc-*co*-MBA hydrogel composition: 20% AAc, 0.15% MBA, 1.5% APS.

the most rapid response was noted over the initial 900 s, followed by a stabilisation of the response as the hydrogel approached equilibrium with the tissue. A control hydrogel was also monitored in the same manner but was not applied to the kiwi surface shows some drift in response, but overall remains relatively stable, indicating water evaporation effects were not significant for these experiments. pH indicator strips were applied to both the outer hydrogel film surface and to kiwi tissue during the experiments (Fig. 7b) to get estimated values of their surface pHs. The outer film surface of the hydrogel interfaced with kiwi tissue showed a gradual pH shift over the experimental timeframe from ~pH 7.0 to 4.0, confirming hydrogen ion diffusion from the acidic tissue into the less acidic environment of the hydrogel over time. The control hydrogel surface maintained a neutral pH of ~7.0 throughout the measurement time (Fig. S9a). The kiwi surface itself remained at ~pH 4.0 for the duration of the experimental time, verifying that the kiwi tissue pH was not being impacted by ion diffusion into the hydrogel, as any surface depletion of ions was likely compensated for from the bulk and thus had a negligible impact on the tissue itself. Dimensional changes of the hydrogel films were also monitored to confirm swelling behaviour with a significant decrease in film dimensions observed for the film interfaced with the kiwi (Fig. 7c), most evident over the initial 600 s. No significant dimension changes were observed in the control hydrogel (Fig. S9b), again indicating that the ion diffusion from the kiwi is driving hydrogel swelling, validating that the impedance response is due to ion diffusion into the hydrogel from the tissue surface and subsequent responsive swelling. This validates the hydrogel's capacity to track pH of underlying tissue in the form of an easily measurable electrical response. This opens up the potential for such hydrogels applicability for real-time, non-invasive

interfacial pH sensing in soft biological environments, highlighting their relevance for wearable biosensor applications.

4. Conclusions

This work establishes electrical impedance spectroscopy as a viable and sensitive method for transducing swelling behaviour in pH-responsive PAAc-*co*-MBA hydrogels, offering significant advantages for wearable biochemical sensing applications. The impedance-based approach demonstrated superior sensitivity to localised hydrogel swelling compared to bulk gravimetric measurements, attributed to the technique's ability to interrogate small volumes near the electrode-hydrogel interface where equilibration occurs more rapidly.

The extracted resistance parameter, R_{gel}, showed excellent correlation with pH-induced swelling and response behaviour dependent on hydrogel formulation. The mechanical investigation of formulation parameters also revealed that hydrogels prepared with lower oxidant concentrations achieved a good balance of mechanical properties combining high elasticity, excellent skin adhesion, and flexibility under dynamic stress. These materials sustained over 350 flexion cycles without failure, demonstrating their suitability for conformal wearable interfaces.

The tissue interface experiments with kiwi fruit provided evidence for the hydrogel's capacity to respond to physiologically relevant pH environments. The progressive decrease in impedance over time, accompanied by measurable dimensional changes and pH mapping, confirmed that hydrogen ion diffusion from acidic tissue drives quantifiable electrical responses in the hydrogel. This represents a significant step towards real-time, non-invasive monitoring of tissue biochemical dynamics. Future work will focus on evaluating swelling–deswelling reversibility, long-term signal stability, and repeated impedance cycling under wearable-relevant conditions, which are important considerations for translating this impedance-based hydrogel sensing platform into practical wearable device applications.

The simplicity of the two-electrode impedance measurement approach, combined with the robust mechanical properties and biocompatible nature of hydrogels, positions this platform as highly promising for integration into next-generation wearable health monitoring devices. The localised sensitivity of impedance measurements offers potential advantages. Future developments will focus on expanding the analytical scope to clinically relevant biomarkers such as lactate, glucose, and inflammatory markers, whilst optimising integration with flexible electronic systems and validating performance under real physiological conditions.

Author contributions

Rinki Singh: conceptualisation, investigation, methodology, formal analysis, and writing – original draft, writing – review & editing. Tanya Levingstone: writing – review & editing. Dinakaran Thirumalai: scientific discussion. Aoife Morrin: supervision, conceptualisation, project administration, writing – review & editing.

Conflicts of interest

There are no conflicts to declare.

Data availability

The majority of the data supporting this article have been included as part of the supplementary information (SI). Additional raw data will be made available upon request. Supplementary information is available. See DOI: https://doi.org/10.1039/d5ma01115a.

Acknowledgements

The authors are grateful to Dublin City University (DCU) for the support of this work. R.S. acknowledges the Irish Research Council for the Government of Ireland Postdoctoral Fellowship (GOIPD/2023/1617) funding. D.T. received funding from the European Union's Horizon 2020 Research and Innovation Programme under the Marie Skłodowska-Curie Grant Agreement No. 101034252.

References

1 H. M. El-Husseiny, E. A. Mady, L. Hamabe, A. Abugomaa, K. Shimada, T. Yoshida, T. Tanaka, A. Yokoi, M. Elbadawy and R. Tanaka, *Mater. Today Bio*, 2022, **13**, 100186.
2 D. R. Seshadri, R. T. Li, J. E. Voos, J. R. Rowbottom, C. M. Alfes, C. A. Zorman and C. K. Drummond, *NPJ Digital Med.*, 2019, **2**, 72.
3 S. Hong, T. Yu, Z. Wang and C. H. Lee, *Biomaterials*, 2025, **314**, 122862.
4 L.-Y. Chu, R. Xie, X.-J. Ju and W. Wang, *Smart hydrogel functional materials*, Springer, 2013.
5 R. Singh and B. Datta, *ACS Appl. Polym. Mater.*, 2023, **5**, 5474–5494.
6 T. Xiang, T. Lu, W.-F. Zhao and C.-S. Zhao, *Langmuir*, 2018, **35**, 1146–1155.
7 H. Mittal, A. Al Alili and S. M. Alhassan, *Microporous Mesoporous Mater.*, 2020, **299**, 110106.
8 S. Kato, Y. Ishiba, M. Takinoue and H. Onoe, *ACS Appl. Bio Mater.*, 2024, **7**, 4093–4101.
9 H. Chenani, M. Saeidi, M. A. Rastkhiz, N. Bolghanabadi, A. H. Aghaii, M. Orouji, A. Hatamie and A. Simchi, *Anal. Chem.*, 2024, **96**, 8160–8183.
10 B. Hu, X. Kang, S. Xu, J. Zhu, L. Yang and C. Jiang, *Anal. Chem.*, 2023, **95**, 3587–3595.
11 L. Fu, A. Yu and G. Lai, *Chemosensors*, 2021, **9**, 282.
12 R. Mahon, Y. Balogun, G. Oluyemi and J. Njuguna, *SN Appl. Sci.*, 2020, **2**, 117.

13 E. Scarpa, V. Mastronardi, F. Guido, L. Algieri, A. Qualtieri, R. Fiammengo, F. Rizzi and M. De Vittorio, *Sci. Rep.*, 2020, **10**, 10854.
14 B. Ahmed, C. F. Reiche, J. J. Magda, F. Solzbacher and J. Körner, *ACS Appl. Polym. Mater.*, 2024, **6**, 5544–5554.
15 X. Wang and X. Wang, *Chem. Commun.*, 2013, **49**, 5957–5959.
16 A. Cubells-Gómez, M. I. Lucío, M.-J. Banuls and Á. Maquieira, *Talanta*, 2024, **279**, 126563.
17 P. Shen, M. Li, R. Li, B. Han, H. Ma, X. Hou, Y. Zhang and J.-J. Wang, *NPG Asia Mater.*, 2022, **14**, 94.
18 S. Calamak, *Microchem. J.*, 2020, **159**, 105473.
19 N. Mac Kenna, P. Calvert and A. Morrin, *Analyst*, 2015, **140**, 3003–3011.
20 N. F. Sheppard Jr, R. C. Tucker and S. Salehi-Had, *Sens. Actuators, B*, 1993, **10**, 73–77.
21 A. Bhat, J. M. Amanor-Boadu and A. Guiseppi-Elie, *ACS Sens.*, 2020, **5**, 500–509.
22 L. V. Whitney, S. Abasi, J. R. Aggas and A. Guiseppi-Elie, *Adv. Sens. Res.*, 2024, **3**, 2300153.
23 H. Kaur, S. S. Siwal, R. V. Saini, N. Singh and V. K. Thakur, *ACS Nanosci. Au*, 2022, **3**, 1–27.
24 C. Daikuzono, C. Delaney, H. Tesfay, L. Florea, O. Oliveira, A. Morrin and D. Diamond, *Analyst*, 2017, **142**, 1133–1139.
25 C. M. Daikuzono, C. Delaney, A. Morrin, D. Diamond, L. Florea and O. N. Oliveira, *Analyst*, 2019, **144**, 2827–2832.
26 K. De Guzman, G. Al-Kharusi, T. Levingstone and A. Morrin, *Anal. Methods*, 2019, **11**, 1460–1468.
27 F. Zhu, B. Mao and J. Yan, *Rev. Anal. Chem.*, 2015, **34**, 87–101.
28 M. Zhang, Q. Yang, K. Liang, L. Gao, P. Lu, C. Ding and Y. Dang, *Polym. Eng. Sci.*, 2023, **63**, 3672–3683.
29 M. Zhong, Y.-T. Liu, X.-Y. Liu, F.-K. Shi, L.-Q. Zhang, M.-F. Zhu and X.-M. Xie, *Soft Matter*, 2016, **12**, 5420–5428.
30 C. Debrie, N. Coudert, J. Abdul, S. Harrisson, O. Colombani and J. Rieger, *Macromolecules*, 2023, **56**, 8497–8506.
31 T. Swift, L. Swanson, M. Geoghegan and S. Rimmer, *Soft Matter*, 2016, **12**, 2542–2549.
32 S. R. Borhade, R. Svensson, P. Brandt, P. Artursson, P. I. Arvidsson and A. Sandström, *ChemMedChem*, 2015, **10**, 455–460.
33 D. J. Panther and S. E. Jacob, *J. Clin. Med.*, 2015, **4**, 970–978.
34 Z. Hu, W. Tang and X. Ji, *Macromol. Rapid Commun.*, 2024, **45**, 2400371.
35 X. Liu, Q. Zhang, Z. Gao, R. Hou and G. Gao, *ACS Appl. Mater. Interfaces*, 2017, **9**, 17645–17652.
36 R. Faturechi, A. Karimi, A. Hashemi, H. Yousefi and M. Navidbakhsh, *Adv. Polym. Technol.*, 2015, 34.
37 X. Zhang, H. Wan, W. Lan, F. Miao, M. Qin, Y. Wei, Y. Hu, Z. Liang and D. Huang, *J. Mech. Behav. Biomed. Mater.*, 2022, **126**, 105044.
38 D. Arunbabu, H. Shahsavan, W. Zhang and B. Zhao, *J. Phys. Chem. B*, 2013, **117**, 441–449.
39 R. Singh, D. Pal and S. Chattopadhyay, *ACS Omega*, 2020, **5**, 21768–21780.
40 K. De Guzman and A. Morrin, *Electroanalysis*, 2017, **29**, 188–196.
41 P. Vadhva, J. Hu, M. J. Johnson, R. Stocker, M. Braglia, D. J. Brett and A. J. Rettie, *ChemElectroChem*, 2021, **8**, 1930–1947.
42 S. Lu, X. Hu, B. Xu, C. Bai, T. Wang, T. Ma and Y. Song, *Food Hydrocolloids*, 2024, **151**, 109799.
43 M. Zhang, S. Hou, Y. Li, S. Hu and P. Yang, *React. Funct. Polym.*, 2022, **170**, 105144.
44 B. Strachota, J. Hodan and L. Matějka, *Eur. Polym. J.*, 2016, **77**, 1–15.
45 B. Strachota, L. Matějka, A. Zhigunov, R. Konefał, J. Spěváček, J. Dybal and R. Puffr, *Soft Matter*, 2015, **11**, 9291–9306.
46 W. Tanan, J. Panichpakdee and S. Saengsuwan, *Eur. Polym. J.*, 2019, **112**, 678–687.
47 Z. Chen, D. Ma, F. Feng and J. Wang, *Sol. Energy Mater. Sol. Cells*, 2024, **266**, 112644.
48 C. Cui, C. Shao, L. Meng and J. Yang, *ACS Appl. Mater. Interfaces*, 2019, **11**, 39228–39237.
49 A. J. Scott, T. A. Duever and A. Penlidis, *Polymer*, 2019, **177**, 214–230.
50 F. Ahmed, J. Song, Masud, S. Lee and J. Kim, *ACS Appl. Polym. Mater.*, 2024, **6**, 13497–13511.
51 C. Chen, Z. Li, S. Chen, L. Kong, Z. Guo, J. Hu, Z. Chen and L. Yang, *J. Mol. Liq.*, 2021, **329**, 115581.
52 S. Bashir, M. Hina, J. Iqbal, A. Rajpar, M. Mujtaba, N. Alghamdi, S. Wageh, K. Ramesh and S. Ramesh, *Polymers*, 2020, **12**, 2702.
53 M. Flinck, S. Kramer and S. Pedersen, *Acta Physiol.*, 2018, **223**, e13068.
54 R. Derwin, D. Patton, P. Avsar, H. Strapp and Z. Moore, *Int. Wound J.*, 2022, **19**, 1397–1408.
55 S. Patel, F. Ershad, M. Zhao, R. R. Isseroff, B. Duan, Y. Zhou, Y. Wang and C. Yu, *Soft Sci.*, 2022, **2**, 9.
56 S. W. Bae, J. S. Lee, V. M. Harms and W. L. Murphy, *Macromol. Biosci.*, 2019, **19**, 1800353.
57 Y. Li, Y. Ma, X. Jiao, T. Li, Z. Lv, C. J. Yang, X. Zhang and Y. Wen, *Nat. Commun.*, 2019, **10**, 1036.
58 S.-J. Jeon, A. W. Hauser and R. C. Hayward, *Acc. Chem. Res.*, 2017, **50**, 161–169.
59 E. H. Choi and H. Kang, *Ann. Dermatol.*, 2023, **36**, 1.
60 K. Wong, P. K. Bhama, J. D. A. Mazimpaka, R. Dusabimana, L. N. Lee and D. A. Shaye, *Am. J. Otolaryngol.*, 2018, **39**, 582–584.
61 A. R. Gonzalez-Navarro, A. Quiroga-Garza, A. S. Acosta-Luna, Y. Salinas-Alvarez, J. H. Martinez-Garza, O. de la Garza-Castro, J. Gutierrez-de la O, D. de la Fuente-Villarreal, R. E. Elizondo-Omaña and S. Guzman-Lopez, *BMC Med. Educ.*, 2021, **21**, 250.
62 Q. Liu, T. Tang, Z. Tian, S. Ding, L. Wang, D. Chen, Z. Wang, W. Zheng, H. Lee and X. Lu, *Nat. Commun.*, 2024, **15**, 6722.